



## Transient modelling of loss and thermal dynamics in power semiconductor devices

Ma, Ke; Yang, Yongheng; Blaabjerg, Frede

*Published in:*

Proceedings of the 2014 IEEE Energy Conversion Congress and Exposition (ECCE)

*DOI (link to publication from Publisher):*

[10.1109/ECCE.2014.6954154](https://doi.org/10.1109/ECCE.2014.6954154)

*Publication date:*

2014

*Document Version*

Early version, also known as pre-print

[Link to publication from Aalborg University](#)

*Citation for published version (APA):*

Ma, K., Yang, Y., & Blaabjerg, F. (2014). Transient modelling of loss and thermal dynamics in power semiconductor devices. In *Proceedings of the 2014 IEEE Energy Conversion Congress and Exposition (ECCE)* (pp. 5495-5501). IEEE Press. <https://doi.org/10.1109/ECCE.2014.6954154>

### General rights

Copyright and moral rights for the publications made accessible in the public portal are retained by the authors and/or other copyright owners and it is a condition of accessing publications that users recognise and abide by the legal requirements associated with these rights.

- Users may download and print one copy of any publication from the public portal for the purpose of private study or research.
- You may not further distribute the material or use it for any profit-making activity or commercial gain
- You may freely distribute the URL identifying the publication in the public portal -

### Take down policy

If you believe that this document breaches copyright please contact us at [vbn@aub.aau.dk](mailto:vbn@aub.aau.dk) providing details, and we will remove access to the work immediately and investigate your claim.

# Transient Modelling of Loss and Thermal Dynamics in Power Semiconductor Devices

Ke Ma, *IEEE Member*, Yongheng Yang, *IEEE Student Member*, Frede Blaabjerg, *IEEE Fellow*

Center of Reliable Power Electronics (CORPE)

Department of Energy Technology

Aalborg University

Pontoppidanstraede 101, Aalborg DK-9220, Denmark

[kema@et.aau.dk](mailto:kema@et.aau.dk), [yoy@et.aau.dk](mailto:yoy@et.aau.dk), [fbl@et.aau.dk](mailto:fbl@et.aau.dk)

**Abstract**—The dynamical behavior of temperature is becoming a critical design consideration for the power electronics, because they are referred as “thermal cycling” which is the root cause of fatigues in the power electronics devices, and thus is closely related to the reliability of the converter. It is well understood that the loading of power devices are disturbed by many factors of the converter system like grid, control, environment, etc., which emerge at various time-constants. However, the corresponding thermal response to these disturbances is still unclear, especially the transient behaviors until achieving the steady-state. As a result, a systematic modelling approach is proposed in this paper, which includes the large signal models of the converter system with both electrical and thermal parts, and the corresponding transient models under frequency domain are also extracted. Based on the proposed models, the bandwidths of the loss or thermal response to major disturbances in the converter system can be analytically mapped, enabling more advanced tools to investigate the transient characteristics of loss and thermal dynamics in the power electronics devices.

## I. INTRODUCTION

Power electronics are being widely used in many important applications of energy conversion like renewable power generations, motor drives, transportations and data center. As a result, the reliability and cost requirements of these power electronics systems are getting more crucial [1]-[3]. As one of the most expensive components and dominant heat sources, thermal issues of power semiconductors are especially important. It has been well known that the loading level of thermal stress in the power device is closely related to the energy conversion efficiency, component ratings, heat sink size, as well as the power density, which all determine the cost of the converter. Moreover, as reported in [4]-[7], the dynamical change of thermal stress in the power device (i.e. temperature swings) is even more problematic because it is one of the most critical causes of failure in power electronics devices. Consequently, correctly modeling the thermal behaviors, especially the transient characteristics of power device temperature is an important step to ensure a reliable and cost-effective converter design [1].

The modelling of complete thermal dynamics in power devices is still a challenging task, as the device loadings are closely related to the mission profiles of the converter, which includes multi-disciplinary models not only for electrical parts, but also for environmental conditions or even mechanical parts. As it is illustrated in Fig. 1, the main

loading disturbances to the power device in a photovoltaic converter system are indicated. It can be seen in Fig. 1 that these disturbances emerge at very different time-constants ranging from microseconds (device switching) to years (ambient temperature changing), resulting in complicated thermal dynamics that is difficult to be predicted. It has been found that the existing loss and thermal models based on time domain seem to be not very suitable to investigate these complicated thermal transients: either very detailed models are applied but restrained to limited time-spans and small time-steps [8], [9], or only the steady-state conditions are in focus with a compromised accuracy of important thermal dynamics [10], [11].

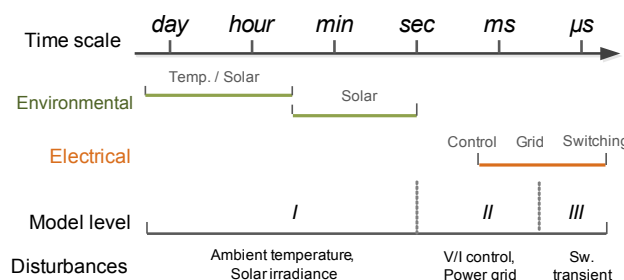


Fig. 1. Typical disturbances to the loading of power devices in a photovoltaic system.

Inspired by the sophisticated frequency-domain analysis in the control and electrical fields [12]-[14], a systematic thermal modelling approach is proposed in this paper. The large signal models of the converter system including both electrical and thermal dynamics are firstly established and correlated. Afterwards, the transfer functions from several critical disturbances to the loss and thermal responses are extracted based on the frequency domain analysis. Finally, the bandwidths as well as response time of the thermal transient caused by several typical disturbances in the converter system are analytically solved.

## II. LARGE SIGNAL MODEL OF WHOLE CONVERTER SYSTEM INCLUDING LOSS AND THERMAL DYNAMICS

A PhotoVoltaic (PV) converter system is chosen to be an example to demonstrate the modelling process in this paper. As it is shown in Fig. 2, the basic structure and configuration of the generator and converter system are illustrated. The

generator system, including the PV panels and the Maximum Power Point Tracking (MPPT) algorithm [15], receives the inputs from the environment disturbances from solar irradiance  $R_{\text{solar}}$  and ambient temperature  $T_{\text{amb}}$ , and then converts them to the PV panel output current  $i_{pv}$  or input current  $i_{in}$  to the converter. Meanwhile, the MPPT algorithm generate a reference DC bus voltage  $v_{dc}^*$  as the control inputs to the converter system [14]. The converter system mainly absorbs the current generated from PV panels, and maintains the DC bus voltage as given by the reference  $v_{dc}^*$  generated from the MPPT. In addition, the current  $i_{abc}$  injected to the grid has to be synchronized with the grid voltage  $E_{abc}$  ( $E_g$ ).

It can be observed in Fig. 2 that the environmental disturbances  $R_{\text{solar}}$  and  $T_{\text{amb}}$  are converted to  $i_{in}$  and  $v_{dc}^*$  as two inputs for the power converter system. The load current injected to the power grid  $i_{abc}$ , as well as the actual DC bus voltage  $v_{dc}$  are the outputs from the converter system. The detailed parameters of the converter are specified in Table I. It should be noted that only the filter inductance is considered for simplicity.

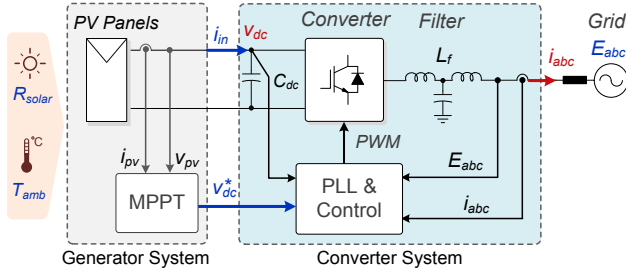


Fig. 2. Configuration of a typical PV generator with single-stage power electronics converter.

TABLE I  
PARAMETERS OF THE CONVERTER SYSTEM FOR A CASE STUDY

Rated DC bus voltage $V_{dc}$	700 V DC
DC capacitance $C_{dc}$	3300 $\mu$ F
Rated power $P_{\text{rated}}$	10 kW
Voltage of grid $E_g$	220 Vrms
Fundamental frequency $f_o$	50 Hz
Switching frequency $f_s$	20 kHz
Filter inductance $L_f$	8.2 mH
Converter topology	3-phase 2-Level
IGBT module (1200V/50A)	FF50R12RT4

After the basic converter application is settled, each part of the converter system can be further modelled. In order to facilitate the transient and frequency domain analysis of the loss/thermal dynamics, a time domain large signal model of the entire conversion system is required, which should not only include the electrical parts of the converter circuit and the control system but also include the thermal parts of the power devices.

#### A. Modelling of Electrical Part

The electrical behaviors of the converter circuit can be represented as three differential equations shown in (1), in which the components in Fig. 2 are represented under the  $dq$  rotational reference frame [14] and the switching cycle average is applied to each of the component [12]. Thereby, a large signal model of the converter circuit can be derived, as it is shown in Fig. 3, where the inputs (blue) and outputs (red) of this model are indicated.

$$\begin{cases} L_F \frac{di_d}{dt} + R_F i_d = \omega L_F \cdot i_q + v_{dc} \cdot d_d - e_d \\ L_F \frac{di_q}{dt} + R_F i_q = -\omega L_F \cdot i_d + v_{dc} \cdot d_q - e_q \\ C_{dc} \frac{dv_{dc}}{dt} = i_{in} - \frac{3}{2}(i_d d_d + i_q d_q) \end{cases} \quad (1)$$

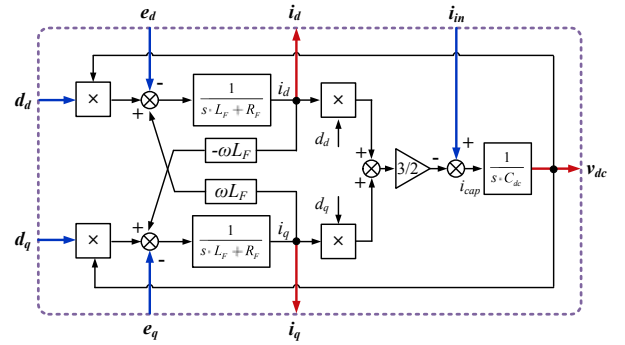


Fig. 3. Large signal model of the converter circuit (blue arrows: inputs of the model; red arrow: outputs of the model; duty ratio  $d_d$  and  $d_q$ ,  $0 \leq d_d \leq 0.5$ ,  $0 \leq d_q \leq 0.5$ ).

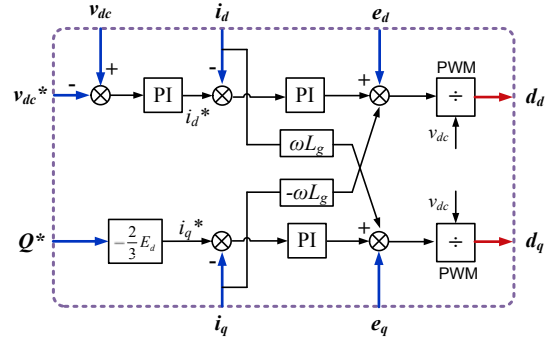


Fig. 4. Large signal model of the control system (blue arrows: inputs of the model; red arrows: outputs of the model).

The control part of the converter system is shown in Fig. 4, where the  $i_d/i_q$  decoupling and the  $e_d/e_q$  feed-forward are employed to improve the control dynamics [14]. A cascaded control structure is applied in the  $d$ -axis with the  $v_{dc}$  control as the outer loop and the  $i_d$  control as the inner loop. The reactive power  $Q^*$  and thus  $i_q$  are normally control as zero in a grid-tied PV converter. Based on Table I, the current Proportional Integrator (PI) controller is tuned with a closed-loop bandwidth of 3.3 kHz ( $K_{P_i} = 102$ ,  $K_{I_i} = 6423$ ), and the voltage PI controller is tuned with a closed-loop bandwidth of 555 Hz ( $K_{P_v} = 9$ ,  $K_{I_v} = 2300$ ).

### B. Modelling of Loss Part

As it has been investigated in [16]-[20], the power losses for the power semiconductor devices are composed of conduction losses and switching losses. When applying the switching cycle average, the conduction losses of power device can be calculated as:

$$P_{\text{cond}@T_H/T_L} = V_{\text{cond}@T_H/T_L}(i_{\text{abc}}) \cdot i_{\text{abc}} \cdot d_{\text{abc}} \quad (2)$$

where  $V_{\text{cond}@T_H/T_L}$  means the conduction voltage for transistor or diode at certain reference junction temperature  $T_H$  or  $T_L$ , and it can be found in the device datasheet or fitted with experimental tests by a function as:

$$V_{\text{cond}@T_H/T_L}(i_{\text{load}}) = V_{\text{cond0}@T_H/T_L} + (i_{\text{load}})^{B_{\text{cond}@T_H/T_L}} \quad (3)$$

The switching losses of power device are calculated as:

$$P_{\text{sw}@T_H/T_L} = f_s \cdot E_{\text{sw}@T_H/T_L}(i_{\text{abc}}) \quad (4)$$

in which  $f_s$  is the switching frequency of the converter,  $E_{\text{sw}@T_H/T_L}$  is the switching energy for transistor or diode at certain reference junction temperature  $T_H$  or  $T_L$ , and it can be also found in the device datasheet or fitted with experimental tests by a function as:

$$E_{\text{sw}@T_H/T_L}(i_{\text{abc}}) = \left(\frac{V_{\text{dc}}}{V_{\text{test}}}\right)^K \left[ S_1 \cdot (i_{\text{abc}})^2 + S_2 \cdot i_{\text{abc}} + S_3 \right] \quad (5)$$

It is known that the loss characteristics of power semiconductor are of temperature dependency [16]-[20]. It is possible to include the junction temperature information into the power loss models. Considering the power loss is linearly distributed with the junction temperature, then the conduction or switching power losses for transistor or diode considering temperature dependency can analytically be solved by:

$$P_{\text{con/sw}@T_j} = \frac{P_{\text{con/sw}@T_H} - P_{\text{con/sw}@T_L}}{T_H - T_L} \cdot (T_j - T_L) + P_{\text{con/sw}@T_L} \quad (6)$$

Then the total losses on transistor or diode can be written as:

$$P_{\text{device}@T_j} = P_{\text{con}@T_j} + P_{\text{sw}@T_j} \quad (7)$$

More details about the loss calculation can be found in [21], and then the large signal model for the device instantaneous loss can be formalized as the diagram shown in Fig. 5.

### C. Modelling of Thermal Impedance Part

As detailed in [22], it has been found that both of the existing Cauer and Foster thermal networks have their limits to acquire the appropriate case temperature of the power device. Consequently, a new thermal model, which combines the advantages of these two thermal networks, is proposed in [22], and it is adopted in this paper.

It can be seen in the thermal model shown in Fig. 6 that the used RC thermal network contains two paths. The first thermal path (*Path 1*) has faster thermal dynamics and is used for the junction temperature estimation. In this path the datasheet-based multilayer Foster thermal network inside

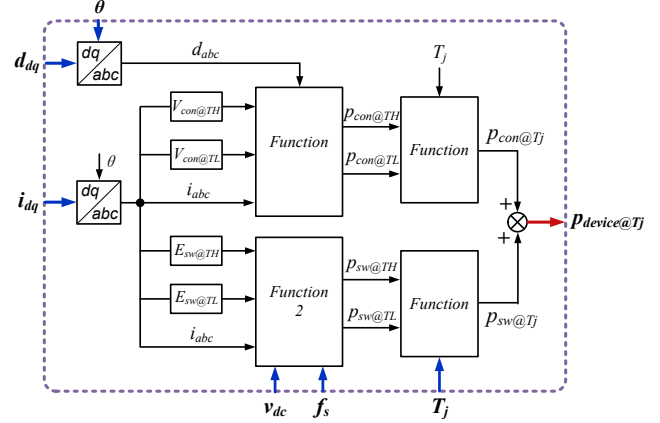


Fig. 5. Large signal model for device loss.

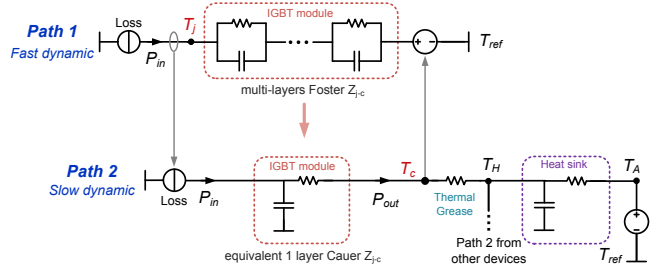


Fig. 6. Used two-path thermal model for power device.

power devices are adopted, and only a temperature potential, whose value is determined by the case temperature  $T_c$  from the other thermal path, is connected to the Foster network. The second thermal path (*Path 2*) has slower thermal dynamics, and is used for the case and heat sink temperature estimations. In this path the thermal network inside the IGBT module is just used for the loss filtering rather than for the junction temperature estimation, and the complete thermal network outside the IGBT module (i.e. thermal grease and heat sink) have to be included. It should be noted that the multi-layer Foster network inside the IGBT module is mathematically transformed to an equivalent single-layer Cauer RC unit ( $Z_{j-c}$ ), which takes the same time to achieve 90 % steady-state junction temperature as the original multi-layer does.

Based on Fig. 6, the large signal model for the device thermal impedance can be also established, it can be formalized as the diagram shown in Fig. 7, where the inputs/outputs are indicated.

### D. Overview of the Whole Converter System for Transient Modelling

When connecting the inputs/outputs of the established large signal models for the control, circuit, loss and thermal parts, the whole converter system can be combined and simplified as the diagram shown in Fig. 8. According to the loss calculations shown in (2)-(7), it is noted that there is no differential function in the large-signal instantaneous loss

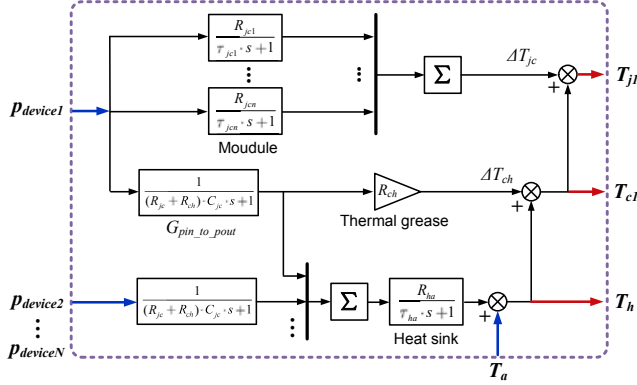


Fig. 7. Large signal model for the thermal impedance shown in Fig. 6.

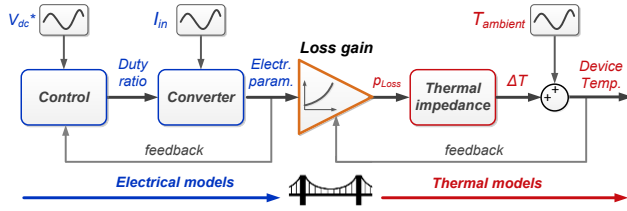


Fig. 8. Overview of the models in an entire PV converter system.

models, and thereby the loss models can be treated as a nonlinear gain without any delays in the signal flow of Fig. 8. As a result, the electrical domain models and thermal domain models can be bridged together, and therefore it is possible to establish the relationship between various disturbances in the converter system to the temperature response in the power devices.

In Fig. 8, the signal propagation and feedbacks can be clearly mapped as follows. Firstly, the control part receives the electrical feedbacks and references to generate the duty ratio for the converter circuit. The circuit model converts the duty ratio to a series of electrical parameters, which can be transferred to the instantaneous power losses  $p_{loss}$  of the device by the loss model. Then, the thermal impedance model transfers the power losses into the temperature rise of the device, by combining the ambient temperature. Finally, the power device temperature can be acquired. It is clear to see that the reference DC bus voltage from the MPPT algorithm  $v_{dc}^*$ , the input current to the converter  $i_{in}$ , and the ambient temperature  $T_{amb}$  (i.e.  $T_{ambient}$  in Fig. 8) are the major disturbances to the device temperature.

### III. FREQUENCY-DOMAIN MODELLING OF THE MAJOR DISTURBANCES TO THE DEVICE LOSS AND THERMAL DYNAMICS

After the large signal models of the whole converter system are established, it is possible to use the frequency domain models to analyze the transient characteristics of both the loss and thermal dynamics. The target is to establish the transfer function from the major thermal disturbances to

the device temperature response. However, because the nonlinear gain of the loss part shown in Fig. 8 is difficult to be linearized, the transfer function is then split into two parts: (a) from major disturbances to the loss related electrical parameters as the first part and (b) from the loss to the device temperature as the second part.

#### A. Transfer Functions in Electrical and Control Parts

When looking at the loss model shown in Fig. 5, the critical parameters in the electrical domain related to power loss of the device are the duty ratio  $d_d$ , the load current  $i_d$  and the DC bus voltage  $v_{dc}$ . By combining and linearizing the circuit and control models shown in Fig. 3 and Fig. 4 respectively, the frequency domain transfer functions of the electrical system can be simplified as the block diagram shown in Fig. 9.

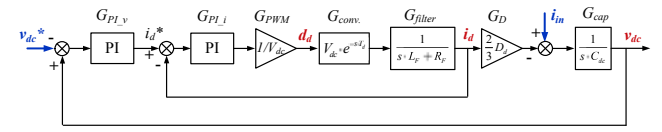


Fig. 9. Complete control diagram combining Fig. 3 and Fig. 4 in frequency domain (blue: disturbances, red: loss-related parameters).

According to Fig. 9, the transfer function from the disturbance  $v_{dc}^*$  to the loss-related parameters  $d_d$ ,  $i_d$  and  $v_{dc}$  can be written as the following three functions in the frequency domain:

$$\frac{d_d(s)}{v_{dc}^*(s)} = \frac{G_{PI_v}(s) \cdot G_{i_d^* d_{d-cl}}(s)}{1 + G_{PI_v}(s) \cdot G_{i_d^* i_{d-cl}}(s) \cdot G_D(s) \cdot G_{cap}(s)} \quad (8)$$

$$\frac{i_d(s)}{v_{dc}^*(s)} = \frac{G_{PI_v}(s) \cdot G_{i_d^* i_{d-cl}}(s)}{1 + G_{PI_v}(s) \cdot G_{i_d^* i_{d-cl}}(s) \cdot G_D(s) \cdot G_{cap}(s)} \quad (9)$$

$$\frac{v_{dc}(s)}{v_{dc}^*(s)} = \frac{G_{PI_v}(s) \cdot G_{i_d^* i_{d-cl}}(s) \cdot G_D(s) \cdot G_{cap}(s)}{1 + G_{PI_v}(s) \cdot G_{i_d^* i_{d-cl}}(s) \cdot G_D(s) \cdot G_{cap}(s)} \quad (10)$$

Similarly, the transfer function from the disturbance  $i_{in}$  to the loss-related parameters  $d_d$ ,  $i_d$  and  $v_{dc}$  can be written as the following three functions in the frequency domain:

$$\frac{d_d(s)}{i_{in}(s)} = \frac{G_{cap}(s) \cdot G_{PI_v}(s) \cdot G_{i_d^* d_{d-cl}}(s)}{1 + G_{cap}(s) \cdot G_{PI_v}(s) \cdot G_{i_d^* i_{d-cl}}(s) \cdot G_D(s)} \quad (11)$$

$$\frac{i_d(s)}{i_{in}(s)} = \frac{G_{cap}(s) \cdot G_{PI_v}(s) \cdot G_{i_d^* i_{d-cl}}(s)}{1 + G_{cap}(s) \cdot G_{PI_v}(s) \cdot G_{i_d^* i_{d-cl}}(s) \cdot G_D(s)} \quad (12)$$

$$\frac{v_{dc}(s)}{i_{in}(s)} = \frac{G_{cap}(s)}{1 + G_{cap}(s) \cdot G_{PI_v}(s) \cdot G_{i_d^* i_{d-cl}}(s) \cdot G_D(s)} \quad (13)$$

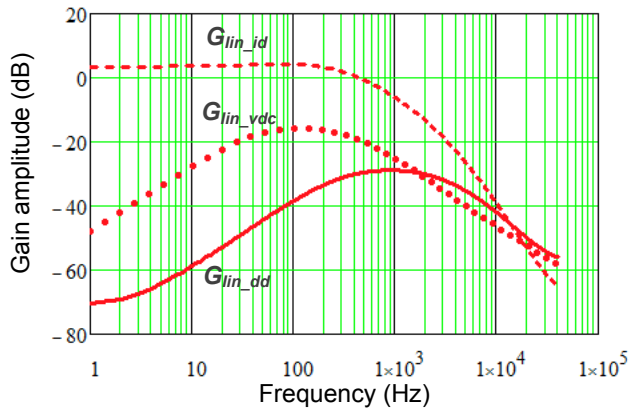
Therefore, the closed-loop transfer functions  $d_d(s)/i_{in}^*(s)$  and  $i_d(s)/i_{in}^*(s)$  can be written as,



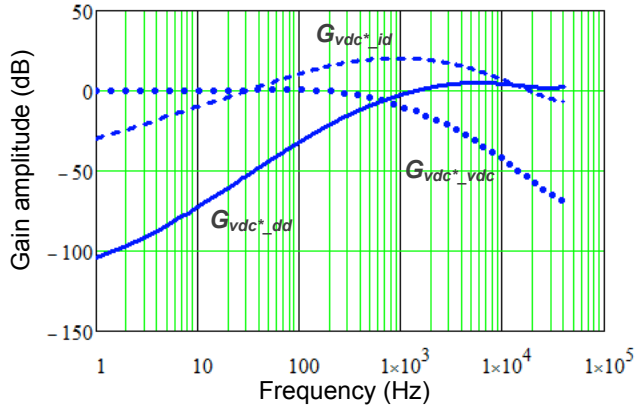
$$G_{i_d^* i_d-cl}(s) = \frac{d_d(s)}{i_d^*(s)} = \frac{G_{PI-i}(s) \cdot G_{PWM}(s)}{1 + G_{PI-i}(s) \cdot G_{PWM}(s) \cdot G_{conv}(s) \cdot G_{filter}(s)} \quad (14)$$

$$G_{i_d^* i_d-cl}(s) = \frac{i_d(s)}{i_d^*(s)} = \frac{G_{PI-i}(s) \cdot G_{PWM}(s) \cdot G_{conv}(s) \cdot G_{filter}(s)}{1 + G_{PI-i}(s) \cdot G_{PWM}(s) \cdot G_{conv}(s) \cdot G_{filter}(s)} \quad (15)$$

Then, Fig. 10 shows the frequency response of the above established transfer functions. It can be seen in Fig. 10 that the disturbances to the electrical parameters has quite different transient characteristics. The corresponding filter type, bandwidth and time domain behaviors in response to step changes of the six established transfer functions are summarized in Table II.



(a)



(b)

Fig. 10. Frequency response of the transfer functions from electrical disturbances to loss-related electrical parameters: (a) disturbance of DC bus input current  $i_{in}$  and (b) disturbance of reference DC bus voltage  $v_{dc}^*$ .

### B. Transfer Function in the Thermal Impedance Part

According to the established thermal impedance model shown in Fig. 7, the transfer function from device power loss  $p_{device}$  to the heat sink temperature  $T_h$ , case temperature

TABLE II  
CHARACTERISTICS SUMMARY OF DIFFERENT DISTURBANCES  
TRANSFER FUNCTIONS (FREQUENCY RESPONSE)

Disturbance	Response	Filter type	Low band (Hz)*	High band (Hz)*	Step response behaviors
$i_{in}$	$d_d$	Band pass	262	2976	Rise and fall
	$i_d$	Low pass	NA	403	Rise
	$v_{dc}$	Band pass	36	384	Rise and fall
$V_{dc}^*$	$d_d$	High pass	1277	NA	Step and fall
	$i_d$	Band pass	262	2976	Rise and fall
	$v_{dc}$	Low pass	NA	403	Rise

\* Frequency when the amplitude has a 3 dB reduction from The maximum amplitude.

$T_c$ , and junction temperature  $T_j$  can be written as the following three functions:

$$G_{p_{device} T_h}(s) = \frac{T_h(s)}{p_{device}(s)} = \frac{1}{(R_{jc} + R_{ch}) \cdot C_{jc} \cdot s + 1} \cdot \frac{R_{ha}}{R_{ha} \cdot C_{ha} \cdot s + 1} = \frac{R_{ha}}{(R_{jc} + R_{ch}) R_{ha} C_{jc} C_{ha} \cdot s^2 + (R_{jc} C_{jc} + R_{ch} C_{jc} + R_{ha} C_{ha}) \cdot s + 1} \quad (16)$$

$$G_{p_{device} T_c}(s) = \frac{T_c(s)}{p_{device}(s)} = \frac{R_{ch}}{(R_{jc} + R_{ch}) \cdot C_{jc} \cdot s + 1} + G_{p_{device} T_h}(s) \quad (17)$$

$$G_{p_{device} T_j}(s) = \frac{T_j(s)}{p_{device}(s)} = \sum_{k=1}^n G_{jc-k}(s) + G_{p_{device} T_c}(s) = \sum_{k=1}^n \frac{R_{jc-k}}{R_{jc-k} C_{jc-k} \cdot s + 1} + G_{p_{device} T_c}(s) \quad (18)$$

Subsequently, the frequency response of the established transfer functions (i.e., (16), (17), and (18)) can be obtained as shown in Fig. 11, where the loss disturbance to the temperature rise  $T_{jc}$  and  $T_{ch}$  are also indicated. Compared to the device temperature levels  $T_j$  and  $T_c$ , the temperature rises of the device  $\Delta T_{jc}$  and  $\Delta T_{ch}$  have relative simpler dynamical behaviors, which can be considered as a lower pass filter.

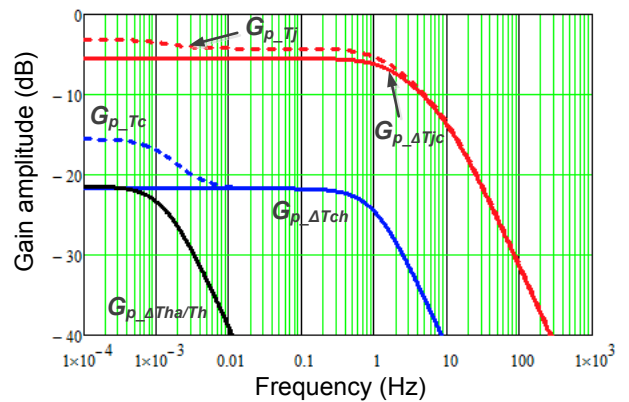


Fig. 11. Frequency response of the transfer functions from the device power loss to the device temperature.

It should be noted that, because the ambient temperature disturbance is directly added to the device temperatures, the transfer function from ambient temperature  $T_{amb}$  to the heat sink temperature  $T_h$ , the case temperature  $T_c$ , and the junction temperature  $T_j$  are equal to one as,

$$\frac{T_h(s)}{T_a(s)} = \frac{T_c(s)}{T_a(s)} = \frac{T_j(s)}{T_a(s)} = 1 \quad (19)$$

#### IV. VALIDATION AND APPLICATION

Based on the acquired bandwidths of various loss and thermal dynamics, the response time ranges of various control, loss and thermal dynamics can be estimated. It is assumed that the equivalent time constant of a transfer function can be calculated by:

$$\tau = \frac{1}{2\pi \cdot \min(f_{bH}, f_{bL})} \quad (20)$$

Then, the time for the transfer function to have a significant response after the disturbance can be calculated as:

$$t_{start} = 0.1\tau \quad (21)$$

Moreover, the time for the transfer function to come into the steady-state after the disturbance can be calculated as:

$$t_{steady} = 2 \times 2.2\tau \quad (22)$$

Then the response time ranges of various control and thermal behaviors to the corresponding disturbances can be calculated and mapped as shown in Fig. 12, in which the parameters can be found in Table III. It is noted that, because the loss is just a nonlinear gain without time delays to the electrical parameters, the response time ranges of power loss should be equal to the control response time.

As it can be seen in Fig. 12, the dynamical response of the loss and thermal behaviors has a clear sequence. Assuming the a disturbance happened at 0 s, the switching transient will first be in progress, and then the electrical parameters as well as power loss start to have a significant response until the steady-state. Finally, the temperature rise of the device will start to respond and require the longest time to achieve the steady-state in the system.

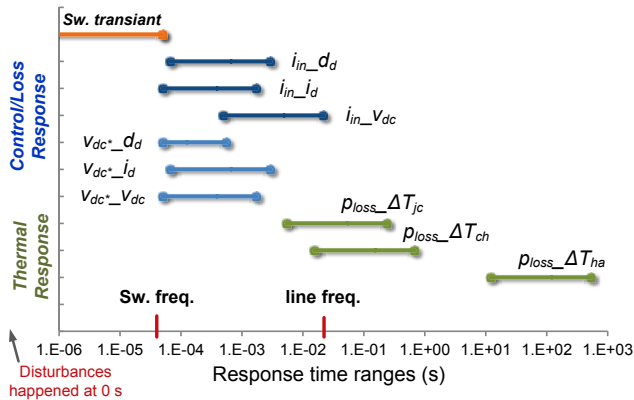


Fig. 12. Calculated time ranges of various responses caused by step disturbances of  $i_{in}$  or  $v_{dc}^*$ .

TABLE III  
TIME PARAMETERS IN FIG. 12

Dis. to Res.	$t_{start}$ (s)	$t_{constant}$ (s)	$t_{steady}$ (s)
$i_{in}$ to $d_d$	6.6e-5	6.6e-4	2.9e-3
$i_{in}$ to $i_d$	5.0e-5	3.9e-4	1.7e-3
$i_{in}$ to $v_{dc}$	4.9e-4	4.9e-3	2.2e-2
$v_{dc}^*$ to $d_d$	5.0e-5	1.3e-4	5.5e-4
$v_{dc}^*$ to $i_d$	6.6e-5	6.6e-4	2.9e-3
$v_{dc}^*$ to $v_{dc}$	5.0e-5	3.9e-4	1.7e-3
$p_{loss}$ to $\Delta T_{jc}$	5.4e-3	5.4e-2	2.4e-1
$p_{loss}$ to $\Delta T_{ch}$	1.5e-2	1.5e-1	6.7e-1
$p_{loss}$ to $\Delta T_{ha}$	1.2e01	1.2e02	5.3e02

In order to validate the analysis for the converter system in terms of transient responses, a time domain simulation is conducted, which is based on the conditions shown in Table I. It is assumed that a step disturbance of the input current  $i_{in}$  happens at 1 s, with an amplitude increase from 0.2 p.u. to 1 p.u. The corresponding electrical and loss dynamics are shown in Fig. 13. It can be seen in Fig. 13 that the dynamical response time ranges of the electrical parameters are in consistency with the calculated values shown in Table III. In addition, the response time of the power loss is the same as that of the electrical parameters (e.g.  $v_{dc}$ ).

Based on the same step disturbance of  $i_{in}$ , the corresponding loss and thermal dynamics are shown in Fig. 14. It can be seen that the response time ranges of the thermal dynamics are also in agreement with the calculated values shown in Table III, which has much longer response time compared to the electrical and loss behaviors.

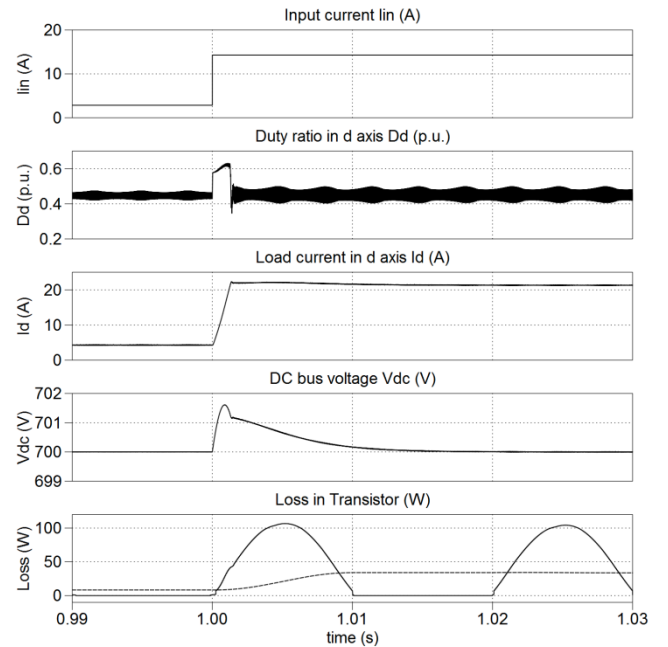


Fig. 13. Time domain simulation of the electrical and loss responses to a step disturbance of  $i_{in}$  (step starts at 1 s).

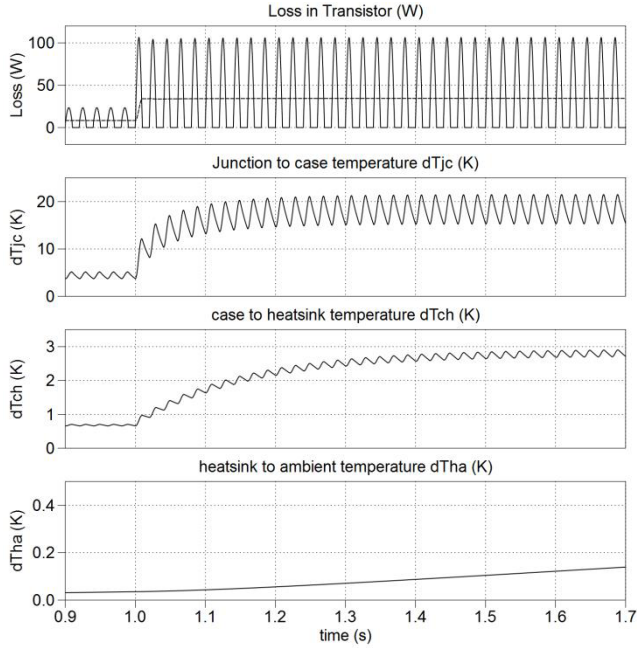


Fig. 14. Time domain simulation of the loss and thermal responses of transistor to a step disturbance of  $i_{in}$  (step starts at 1 s).

## V. CONCLUSIONS

A systematic modelling approach has been proposed in this paper, which includes the large signal models of the converter system with both electrical and thermal parts. The corresponding transient behavior models in the frequency domain are also extracted, which enables a transient analysis of both power losses and thermal dynamics in the power semiconductor devices. Based on the proposed models, the bandwidths of the loss and the thermal response to the major disturbances in the power converter system can be analytically mapped, and consequently, more advanced tools to investigate the transient characteristics of loss and thermal dynamics in the power electronics devices can be developed. A case study on a 10 kW single-stage grid-connected PV inverter system has been adopted to illustrate the application of the proposed systematic modelling approach. The results have demonstrated that, the models established in this paper can effectively reflect both the steady-state and transient behaviors of the converter circuit, the control system, and the power devices (losses and temperature), which thus can be adopted for the design of reliable and robust power electronics converter systems.

## REFERENCES

- [1] F. Blaabjerg and K. Ma, "Future on power electronics for wind turbine systems," *IEEE Journal of Emerging and Selected Topics in Power Electronics*, vol. 1, no. 3, pp. 139-152, 2013.
- [2] Z. Chen, J.M. Guerrero, and F. Blaabjerg, "A review of the state of the art of power electronics for wind turbines," *IEEE Trans. Power Electron.*, vol. 24, no. 8, pp. 1859-1875, Aug. 2009.
- [3] S. Faulstich, P. Lyding, B. Hahn, and P. Tavner "Reliability of offshore turbines—identifying the risk by onshore experience," in *Proc. of European Offshore Wind*, Stockholm, 2009.
- [4] C. Busca, R. Teodorescu, F. Blaabjerg, S. Munk-Nielsen, L. Helle, T. Abeyasekera, and P. Rodriguez, "An overview of the reliability prediction related aspects of high power IGBTs in wind power applications," *Microelectronics Reliability*, vol. 51, no. 9-11, pp. 1903-1907, 2011.
- [5] E. Wolfgang, "Examples for failures in power electronics systems," presentation at *ECPE Tutorial on Reliability of Power Electronic Systems*, Nuremberg, Germany, Apr. 2007.
- [6] S. Yang, A. T. Bryant, P. A. Mawby, D. Xiang, L. Ran, and P. Tavner, "An industry-based survey of reliability in power electronic converters," *IEEE Trans. Ind. Appl.*, vol. 47, no. 3, pp. 1441-1451, May/Jun. 2011.
- [7] J. Due, S. Munk-Nielsen, and Rasmus Nielsen, "Lifetime investigation of high power IGBT modules," in *Proc. of EPE'11*, Birmingham, 2011.
- [8] D. Hirschmann, D. Tissen, S. Schroder, and R.W. De Doncker, "Inverter design for hybrid electrical vehicles considering mission profiles," in *Proc. of the IEEE Conference on Vehicle Power and Propulsion*, pp. 1-6, Sept. 7-9, 2005.
- [9] H. Wang, K. Ma, and F. Blaabjerg, "Design for reliability of power electronic systems," *Proc. of IECON'2012*, pp. 33-44, 2012.
- [10] O.S. Senturk, S. Munk-Nielsen, R. Teodorescu, L. Helle, and P. Rodriguez, "Electro-thermal modeling for junction temperature cycling-based lifetime prediction of a press-pack IGBT 3L-NPC-VSC applied to large wind turbines," in *Proc. of ECCE'2011*, pp. 568-575, 2011.
- [11] K. Ma, F. Blaabjerg, and M. Liserre, "Thermal Analysis of Multilevel Grid Side Converters for 10 MW Wind Turbines under Low Voltage Ride Through," *IEEE Trans. Ind. Appl.*, vol. 49, no. 2, pp. 909-921, 2013.
- [12] S. Bacha, L. Munteanu, and A.L. Bratcu, *Power Electronics Converters modelling and Control*, Springer, 2014.
- [13] M. Liserre, F. Blaabjerg, and S. Hansen, "Design and control of an LCL-filter-based three-phase active rectifier," *IEEE Trans. Ind. Appl.*, vol. 41, no. 5, pp. 1281-1291, 2005.
- [14] R. Teodorescu, M. Liserre, and P. Rodriguez, *Grid Converters for Photovoltaic and Wind Power Systems*, Wiley-IEEE press, 2011.
- [15] T. Esram and P.L. Chapman, "Comparison of photovoltaic array maximum power point tracking techniques," *IEEE Trans. Energy Convers.*, vol. 22, no. 2, pp. 439-449, 2007.
- [16] S. Dieckerhoff, S. Bernet, and D. Krug, "Power loss-oriented evaluation of high voltage IGBTs and multilevel converters in transformerless traction applications," *IEEE Trans. Power Electron.*, vol. 20, no. 6, pp. 1328-1336, Nov. 2005.
- [17] F. Blaabjerg, U. Jaeger, S. Munk-Nielsen, and J. Pedersen, "Power Losses in PWM-VSI Inverter Using NPT or PT IGBT Devices," *IEEE Trans. Power Electron.*, vol. 10, no. 3, pp. 358-367, May 1995.
- [18] M.H. Bierhoff and F.W. Fuchs, "Semiconductor losses in voltage source and current source IGBT converters based on analytical derivation," in *Proc. of PESC'2004*, pp. 2836-2842, 2004.
- [19] O.S. Senturk, L. Helle, S. Munk-Nielsen, P. Rodriguez, and R. Teodorescu, "Power capability investigation based on electrothermal models of press-pack IGBT three-level NPC and ANPC VSCs for multi-megawatt wind turbines," *IEEE Trans. Power Electron.*, vol. 27, no. 7, pp. 3195-3206, 2012.
- [20] I. Swan, A. Bryant, P.A. Mawby, T. Ueta, T. Nishijima, and K. Hamada, "A fast loss and temperature simulation method for power converters, Part II: 3-D thermal model of power module," *IEEE Trans. Power Electron.*, vol. 27, no. 1, pp. 258-268, 2012.
- [21] K. Ma, A.S. Bahman, S.M. Beczkowski, and F. Blaabjerg, "Loss and thermal model for power semiconductors including device rating information," in *Proc. of IPEC'2014*, Japan, 2014.
- [22] K. Ma, F. Blaabjerg, and M. Liserre, "Electro-thermal model of power semiconductors dedicated for both case and junction temperature estimation," in *Proc. of PCIM'13*, pp. 1042-1046, 2013.